



---

# ANAMOLY OF BERRYLIUM

---

Post M.Sc Project - 2017

Submitted to:

Prof. Manoj Sharan (HENPP)

Prof. Bijay Agrawal (Theory Division)

SUBMITTED BY:

RASHIKA GUPTA  
Post M.Sc – 2017  
June 27 '2018.

## **ACKNOWLEDGEMENT**

I would like to express my sincere gratitude to my guide and co-guide Prof. Manoj Sharan and Prof. Bijay Agrawal who have helped me through; regular discussions, enthusiasm to work and immense knowledge that both have was really beneficial. I would like to thank them for all the suggestions and co-operation.

I would also like to express my gratitude to VECC staff: Ganesha Da, Partha Sir, Ramnarayan Sir without whose support this project would not have been successful. I would also like to take this opportunity to thank my friends and senior who have been a constant support and been my venting machine.

## **CONTENTS:**

- 1.** Introduction
- 2.** Motivation
- 3.** Experimental Setup and Measurements
- 4.** Observation
- 5.** Conclusion
- 6.** Plans
- 7.** Reference

# 1.INTRODUCTION

In the 19<sup>th</sup> century, all around the globe physicist were discovering the particles that helped in explaining the forces of the nature. Beginning from the discovery of the electrons to the discovery of the higgs boson in 2012. These elementary particles describe the standard model i.e the theory describing the four fundamental forces (i.e the electromagnetic interaction, the weak interaction and the strong nuclear interaction; the fourth one being the Gravitational force). Although, the standard model is a self – consistent theory, it still doesn't incorporate for the theory of gravity, neutrino oscillations and existence of the dark matter. Hence, a fundamental fifth force is proposed which will explain all such anomalous observations that do not fit the theories as of now.

One such experiment conducted by ATOMKI group \*\*\*\*\* details\*\*\*\*\* claims to have get hold of the new particle in nuclear physics experiment. This has astonished everyone around the community as the group asserts it to be a light boson particle which is 34 times heavier than the electron. The decay of an excited state of the  $^8\text{Be}$  to its ground state leads to the production of a boson which further decays to electron and positron pair during the transition.  $^8\text{Be}$  has always been of an interest to explore more about the nuclear structure it constitutes 4 protons and 4 neutrons.

It is therefore interesting to investigate the study of  $^8\text{Be}$  nuclei. In this experiment, we are interested in the following states of the nuclei:

State	Energy (MeV)	Width(keV)	$J^P$	Isospin
$^8\text{Be}^*$	18.15	138	1+	0
$^8\text{Be}^{**}$	17.64	10.7	1+	1
G.S	0		0+	0

Table 1

The excited states majorly decay promptly to  $^7\text{Li}$ , but also through the emission of gamma ray or a virtual photon produced from electron positron pair; this process is called internal pair conversion. In an IPC, a nucleus emits an  $e^-e^+$  pair instead of the gamma ray quantum. Along with the emitting nuclei and the  $e^-e^+$  pair it forms a three-body decay [3]. It usually decays with a small opening angle between  $e^-e^+$ . It is in this process that there is an oddity.

The  $^8\text{Be}$  decay anomaly: In the experiment by ATOMKI group, to populate the 17.6 MeV and 18.15 MeV 1+ states,  $^7\text{Li}(p, \gamma)^8\text{Be}$  reaction was performed using the proton beam of energies 0.441 MeV and 1.03 MeV were used as shown in fig 1. Since, the separation energy of the proton from  $^8\text{Be}$  is 1.725 MeV the energy difference between the separation energy is .385 MeV and 0.895 MeV for first and second excited state as shown in the table 1 in the center of mass frame. Energy of proton in the lab frame to populate the first excited state and second excited state is therefore: 0.44 MeV and 1.023 MeV which matches with the experimental values. Essentially, the proton of these energies excites  $^7\text{Li}$  to excited state of  $^8\text{Be}$ . The energy of proton is chosen to be this as it helps in producing one excited state and is not contaminated from decays of other excited states. Also, since these states are produced in the resonance; therefore, there is a high yield of these excited states. The excited states decay to the ground state from  $^8\text{Be}^*$  to the ground state through an emission of electron positron pair via M1 transition (since, there is no change in the parity and change in

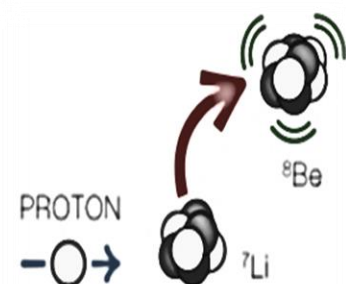


Fig. 1

$J=1$ ). These emission of  $e^-e^+$  pair were detected by  $d\Delta\Delta - E$  detector setup as shown in fig 2

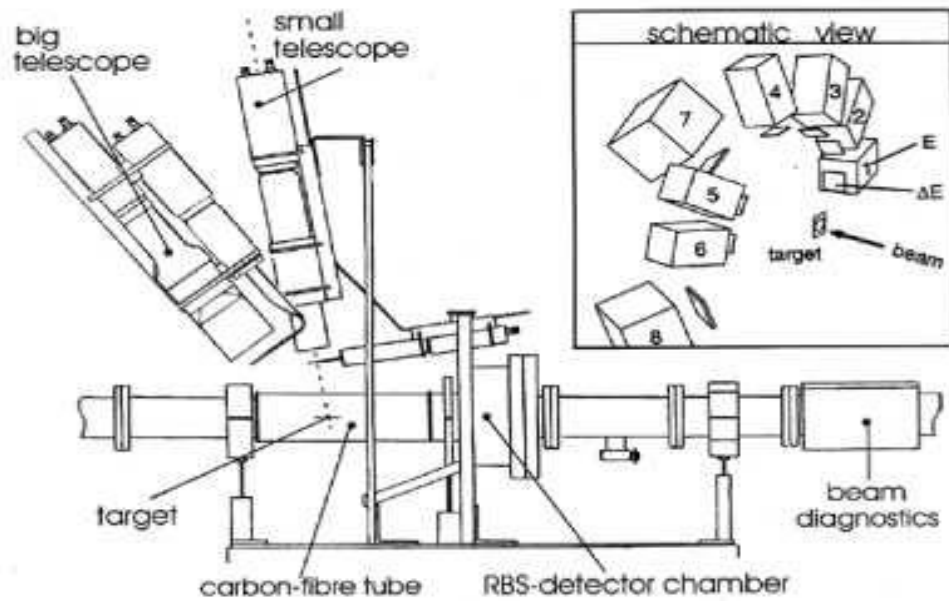


Fig 2 Experimental Setup: Schematic Diagram

It consists of six detector telescopes mounted at fixed positions allowing observation of 15 co-relation angles [3]. Each detector consisting of  $\Delta E$  – detector of the dimensions :  $2.2 * 2.2 \text{ cm}^2$  of thickness 0.1 cm and; E detector of dimension:  $3.0 * 3.0 \text{ cm}^2$  and thickness 7 cm in an attempt to maximize the solid angle coverage[ 3]. The detectors were placed at perpendicular to the beam direction at angle of 0 deg, 60 deg, 120 deg, 180 deg, and 270 deg as shown in fig 3. These angles ensured the homogenous acceptance of  $e^+e^-$  pairs as a function of co-relation angle. It is noted from the literature that in the energy region of our interest the energy loss of the electrons (of 5 MeV – 20 MeV) is roughly constant. For better statistics, the angular correlations were done in the coincidence to suppress the single gamma events.



Fig 3. Experimental Setup by ATOMSKI

In this transition, most of the electron–positron pairs have small opening angle with a smoothly decreasing number as with larger opening angles as it is planar three-body decay. One expects it to be shown in fig 4(left) for ordinary nuclear transition except for E0 transitions. In  $^8\text{Be}$  M1 transition occurs from both the excited states of 17.6 MeV and 18.15 MeV. In contrast, the angular co-relations became sharply peaked at larger angles as shown in fig 4 (right). The discrepancy from the expectations can be

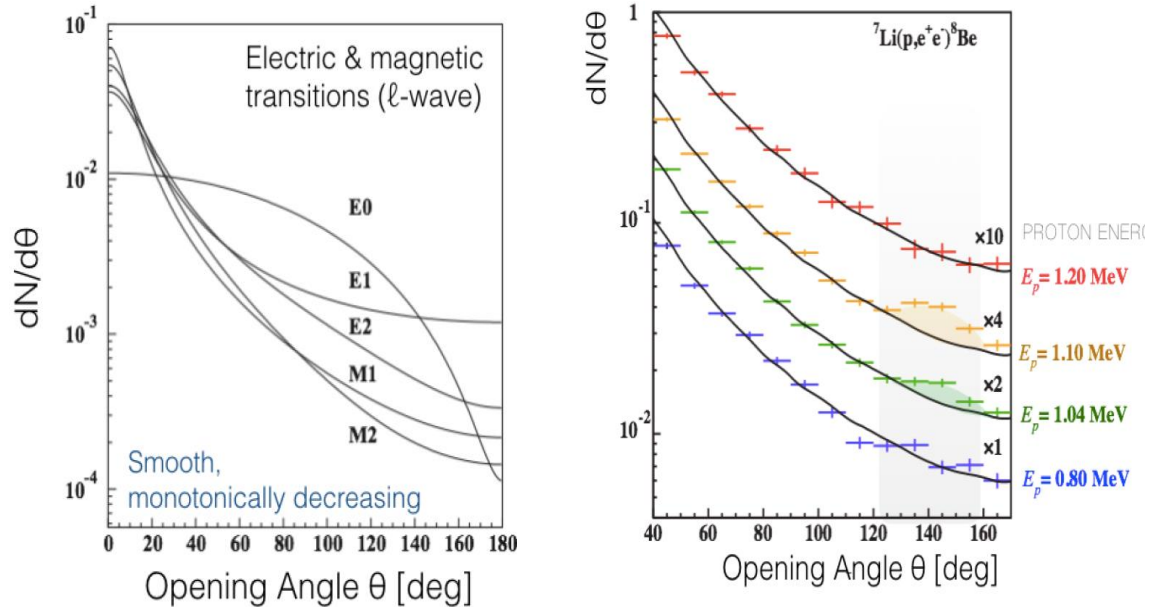
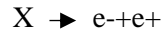


Fig 4

explained by unidentified nuclear transitions or some contribution from the experimental effects, but the observed distribution can be beautifully explained by assuming the production of a boson, X[2]. If the nucleus emits a neutral boson, instead of IPC it happens by two-body decay. The boson decaying through  $e^-e^+$  pair is again 2 – body decay i.e



in centre of mass system[3]. While, in the laboratory frame the momentum of the boson makes this angle equivalent to angle smaller than 180 deg but the angular distribution from IPC which helps in explaining the bump at higher angles around 140 deg with a significance factor  $> 5$  sigma since in the laboratory frame the boson is produced with  $v = 0.35c$ [2]. The invariant mass  $m_X$  of the boson, the positron and the electron momenta  $p_+$  and  $p_-$  and their energies  $E_+$  and  $E_-$  are related by the given formula by conserving the energy:

$$M_X^2 = 2m_e^2 + 2 E_+ E_- - 2 p_+ p_- \cos \theta \text{ or,}$$

This relates the mass of new particle in terms of the opening angle and energies of electron and positron.

Understanding the transitions: Earlier, an experiment was performed by de Boer et al[4] at University of Frankfurt. They performed measurement of IPC of nuclear transition of 17.2 MeV with  $J^\pi = 1^-$  and iso-spin = 1; which is similar to M1 decay of 17.6 MeV in  $^8\text{Be}$ . The  $^{12}\text{C}$  resonance at 17.2 MeV with a width of 1.15 MeV was populated in the  $^{11}\text{B}(p, \gamma)^{12}\text{C}$  reaction with  $E_p = 1.6$  MeV. It decays to ground state by isovector E1 transition. It is important to note that both the nuclei of these energies are well suited for the comparative study. They both have the same energy, required the same target condition and same experimental setup. Following the same technique, the co-relation angle distribution was plotted with respect to the ratio of yield of pairs to IPC (prediction). The following curves were observed:

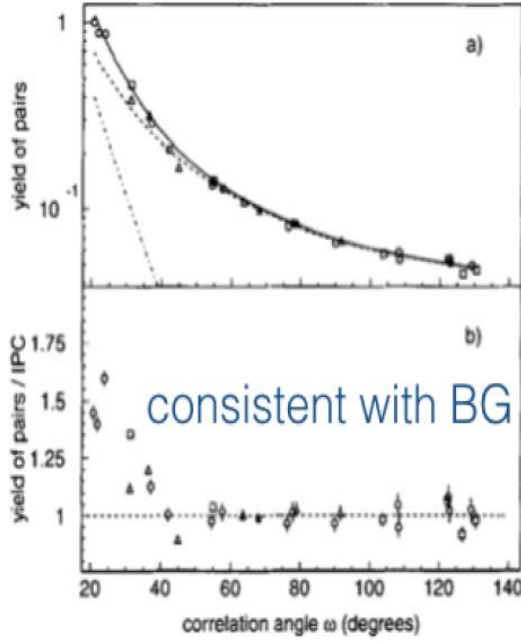


Fig 5

It was observed that the ratio of data and IPC obtained shows good agreement with the expectations; as shown by the flat “signal– background” on the bottom panel in fig 5. In fig 6, the same analysis for the M1 is shown for  $^8\text{Be}$ . The “signal – background” now shows a broad excess across all opening angles. This made the Institute of Nuclear Physics group of Frankfurt to postulate a short lived boson of masses between 5 and 15 MeV. Since, there was no deviation in IPC in  $^{12}\text{C}$  for large angle but was observed for M1 decay in  $^8\text{Be}$  with 4.5 standard deviation.

Later, when ATOMKI group performed the same experiment and observed both the transition from states of 17.6 MeV and 18.15 MeV as mentioned in table 1, they found that the deviation in correlation angle for M1 decay of 17.6 MeV could be explained from the mixing of some E1 component which is coming from the direct (non resonant) proton capture whose multipolarity is dominantly E1 [5] which depends on the target thickness as well as the width of the excited state. as shown in fig 7. However, they also measured the correlation

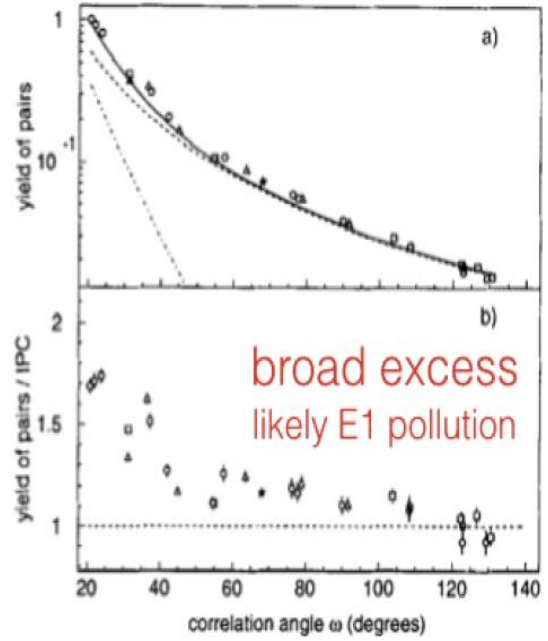


Fig 6

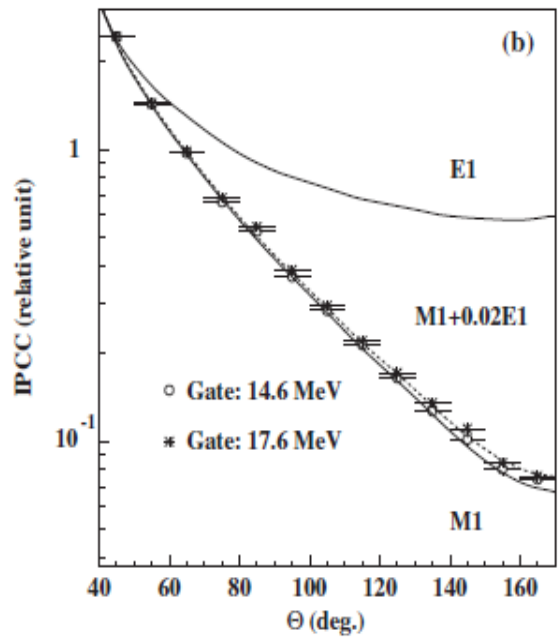


fig 7

angle of  $e^-e^+$  originated from the 18.15 MeV transition and compared with the simulated ones (full curves) assuming M1+ E1 transitions with some mixing ratios. It was observed that 18.15 MeV resonance state decaying through isoscalar M1 transition showed the excess is concentrated in the bump for angles around 140 deg as shown in fig 6 [1]. These observations could possibly from the nuclear interference or might be because of an intermediating particle produces, a neutral isoscalar particle with mass 16.7 MeV being created.

## **2.MOTIVATION**

There are various studies done on the low mass nuclei of mass 8-10 but mostly through the decay of alpha particles or gamma decay. There are very few measurements of angle correlation of  $e^-e^+$  pair from internal pair conversion.

Following from the experimental results of the ATOMKI group and the Frankfurt group; it will be interesting to investigate the decay of  $^8\text{Be}$  nuclei populated around 18 MeV. It is important to narrow down on what factors does the deviation in the correlation angle occurs; whether it is isoscalar or isovector transition. Though, from both the experiments it is clear that the bump is extensively observed in the M1 transition from the  $^8\text{Be}$  and there is IPC (Internal Pair Conversion) transition in the E1 decay of the  $^{12}\text{C}$  excited state of 17.2 MeV. Typically, the branching ratio of IPC is very small. Therefore, it will be challenging to measure the  $e^-e^+$  pair suppressing all the backgrounds gamma rays.

It is necessary to make an experimental setup with good detection efficiency of detecting the  $e^-e^+$  pairs along with a better resolution so as to analysis it more effectively.



### **3.MEASUREMENTS AND EXPERIMENTAL STATUS:**

In the present project, as noted from the literature survey it is important to understand the nuclear structure of  $^8\text{Be}$  and similar nuclei like it. It follows that other nuclei like  $^{10}\text{B}$ ,  $^{10}\text{Be}$   $^{12}\text{C}$  will be interesting to analyse and understand better.

In order to understand the nuclear structure and transition that follows we need to know the constituents of nuclei (the nucleons, that is, protons and neutrons) and treat them as QM objects. From the point of view of QM, one must know what is the state of the system (at equilibrium). Thus, we want to solve the time-independent Schrödinger equation. This gives us the energy levels of the nuclei. The exact nature of the forces that keep together the nucleus constituents are the study of quantum chromodynamics, which describes and look for the source of the strong interaction. As of now, it is beyond this project to explore that.

#### **3.1. Experimental Setup**

As seen from the literature survey, the experiment has to be done more precisely. Since, we are looking at the low energies; the detector used should be able to resolve and be efficient. We are primarily looking for  $e^-$  and  $e^+$  pair. Their energy deposition and the angular distribution will help us in identifying the properties. This will solve the mystery of the unknown light boson.

#### **3.2. DETECTION TECHNIQUE - SCINTILLATOR**

Scintillation is a flash of light produced in a transparent material by the passage of a particle (an electron, an alpha particle, an ion, or a high-energy photon). This helps in detection of any charged particle passing through it. The ideal scintillation material should possess the following properties:

1. It should convert the kinetic energy of charged particles into detectable light with high scintillation efficiency.
2. This conversion should be linear-the light yield should be proportional to deposited energy over as wide a range as possible.
3. The medium should be transparent to the wavelength of its own emission for good light collection.
4. The decay time of the induced luminescence should be short so that fast signal pulses can be generated.
5. The material should be of good optical quality and subject to manufacture in sizes large enough to be of interest as a practical detector.
6. Its index of refraction should be near that of glass to permit efficient coupling of the scintillation light to a photomultiplier tube or other light sensor.

No material simultaneously meets all these criteria, and the choice of a particular scintillator is always a compromise among these and other factors. There are different types of scintillators such as inorganic alkali halide crystals and organic based liquids and plastics scintillators. The inorganics tend to have the best light output and linearity, but with several exceptions are relatively slow in their response time. Organic scintillators are generally faster but yield less light. The intended application plays an important role in choosing the type of scintillator. In the following section, the organic scintillator is discussed and a type of organic scintillator – plastic scintillator used during the experiment.

## ORGANIC SCINTILLATOR

a) **Mechanism:** The process of the prompt emission (fluorescence) of the visible radiation from a molecule because of the excitation process in organics arises from transitions in the energy level structure of a single molecule. It can be observed from a given molecular species independent of its physical state. A large category of practical organic scintillators is based on organic molecules with certain symmetry properties that give rise to what is known as a pie-electron structure. Energy can be absorbed by exciting the electron configuration into any one of a number of excited states. A series of singlet states (spin 0) are labeled as  $S_0$ ,  $S_1$ ,  $S_2$ . A similar set of triplet (spin 1) electronic levels are also shown as  $T_1$ ,  $T_2$ ,  $T_3$ . In the organic scintillators, the energy spacing between  $S_0$  and  $S_1$  is 3 or 4 eV, whereas spacing between higher-lying states is usually somewhat smaller. Each of these electronic configurations is further subdivided into a series of levels with much finer spacing that correspond to various vibrational states of the molecule. Typical spacing of these levels is of the order of 0.15 eV which is less than the average thermal energies. A second

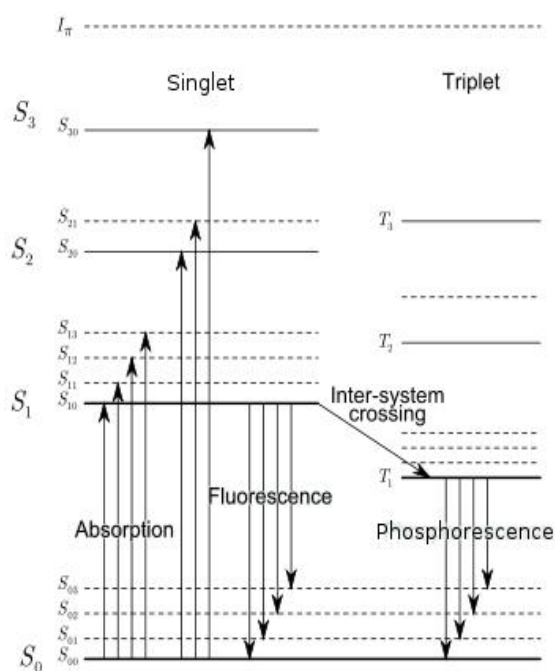


Fig 8

subscript is often added to distinguish these vibrational states, and the symbol  $S_{00}$  represents the lowest vibrational state of the ground electronic state.

In the case of a scintillator, because of the kinetic energy a charged particle it gets absorbed. The higher singlet electronic states that are excited are quickly (on the order of picoseconds) de-excited to the  $S_1$  electron state through radiationless internally. The excess vibrational energy of the  $S_{11}$  and  $S_{12}$  which is not in thermal equilibrium with its neighbors quickly loses this energy. Therefore, the net effect of the excitation process in a simple organic crystal is to produce, after a negligibly short time period, a population of excited molecules in the  $S_{10}$  state. The principal scintillation light (or prompt fluorescence) is emitted in transitions between this  $S_{10}$  state and one of the vibrational states of the ground electronic state. The lifetime for the first triplet state  $T_1$  is characteristically much longer than that of the singlet state  $S_1$  and the radiation emitted in a de-excitation from  $T_1$  to  $S_0$  is therefore a delayed light emission. Because  $T_1$  lies below  $S_1$ , the wavelength of this phosphorescence spectrum will be longer than that for the fluorescence spectrum. While in the  $T_1$  state, some molecules may be thermally excited back to the  $S_1$  state and subsequently decay through normal fluorescence. This represents the origin of the delayed fluorescence sometimes observed for organics which explains why they are transparent to their own fluorescence emission.

## PLASTIC SCINTILLATOR

For years, plastic scintillator is used for particle physics measurements owing to its special characteristics. When an organic scintillator is dissolved in a solvent that can then be subsequently polymerized, the equivalent of a solid solution can be produced.

A common example is a solvent consisting of monomer in which an appropriate organic scintillator is dissolved. The monomer is then polymerized to form a solid plastic. Because of the ease with which they can be shaped and fabricated, plastics have become an extremely useful form of organic scintillator. In the present project, we have used Polyvinyl Toluene.

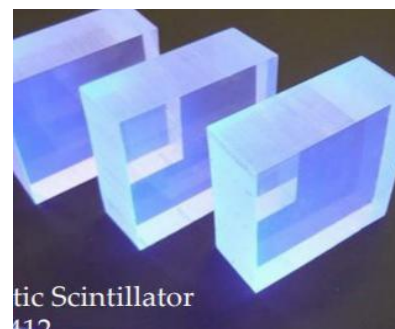


Fig 9

Plastic scintillators are available commercially with a good selection of standard sizes of rods, cylinders, and flat sheets. Since, the material is relatively inexpensive and has better performance, plastics are often the only practical choice if large-volume solid scintillators are needed. The advantages of plastic scintillators include fairly high light output and a relatively quick signal, with a decay time of 2–4 nanoseconds.

In the current project, we are interested in studying the electron positron pair and want to avoid the gamma rays coming from the background; plastic scintillator helps us with this. Because of low  $Z$ , gamma interacts less with the molecules when compared to the inorganic scintillator. Consequently, it detects the  $e^-e^+$  pairs more efficiently compared to the gamma rays which is also later shown. Its compact size will be beneficial to us for making a large array which is required for the experiment so as to cover the maximum solid angle.

3.3 After getting a signal from the detector, it has to be amplified or converted to a significant signal. For this purpose, an attempt was made to make the prototype using different type of the multipliers:

1. Photomultiplier: A photomultiplier tube, useful for light detection of very weak signals, is a photoemissive device in which the absorption of a photon results in the emission of an electron. These detectors work by amplifying the electrons generated by a photocathode exposed to a photon flux.[fsu pmt]. It has been already discussed widely in the previous project. A plastic scintillator detector was designed by us and along with it a photomultiplier tube is attached to it as shown in the fig: \*\*

2. We plan to also make a prototype using Silicon Photomultiplier (SiPM). It is a solid-state photodetector that in response of a photon can produce a current pulse several tens nanoseconds long with almost million electrons. It has a gain which is comparable to the PMT.

A photodiode is formed by a silicon p-n junction that creates a depletion region that is free of mobile charge carriers. When a photon is absorbed in silicon it creates an electron-hole pair. Applying a reverse bias to a photodiode sets up an electric field across the depletion region that causes these charge carriers to be accelerated towards the anode (holes), or cathode (electrons). Therefore, an absorbed photon will result in a net flow of current in a reverse-biased photodiode. When a sufficiently high electric field ( $> 5 \times 10^5$  V/cm) is generated within the depletion region of the silicon (achieved by the sensor design and application of a recommended bias), a charge carrier created there will be accelerated to a point where it carries sufficient kinetic energy to create secondary charge pairs through a process called impact ionization. In this way, a single absorbed photon can trigger a self-perpetuating ionization cascade that will spread throughout the silicon volume subjected to the electric field. The silicon will break down and become conductive, effectively amplifying the original electron-hole pair into a macroscopic current flow. This process is called Geiger discharge, in analogy to the ionization discharge observed in a Geiger- Müller tube.

When compared with the PMT, SiPM not only combines the low-light detection capabilities of the PMT but also provides other benefits as mentioned below:

1. It operates in the low voltage (PMT  $\sim 1$  kV), in the order of 50V.
2. Since there is no electric field in it; it is insensitive to the magnetic fields. It is one of the major characteristic of SiPM which will be explored in the project. We are interested in detecting the  $e^-e^+$  pair which have almost the same properties other than the charge. It will be important to differentiate between both the charges for which we plan to apply the magnetic field in the detection system. This will just change the trajectories of the pair and do nothing else while making it simpler for us to detect. This kind of set-up won't be possible if we use the PMT which might behave differently when an external magnetic field is applied.
3. It is robust and has excellent uniformity of response.

In the project, we have tried to understand the characteristic of the SiPM and determined the breaking voltage and different operating voltage. Some spectra were obtained as discussed in the next section.

Alongwith, the benefits of using SiPM there are some limitations which should be kept in mind while operating them. It is temperature sensitive (since, it is essentially a diode) therefore, a temperature controller should be used while using it. It will be also shown in the graph that it depends on the voltage that it is operated at. One must wisely choose and fix the voltage while using it.

#### Use of $\Delta E$ - E detectors- Telescope Method:

After one finalizes which prototype provides us with better result. They have to made of different thickness and have to arranged in a particular. Usually, to identify the kind of the charged particle one uses  $\Delta E$  – E telescope method. It consists of the one very thin detectors and one thick detector. Particle pass through the delta E detector and lose their part of energy in it. While the thicker detector stops the particle. The energy lost and energy deposited helps in the identification of the particle. Though things may be different for the lower energy particles, where it is likely possible that the particle might stop.

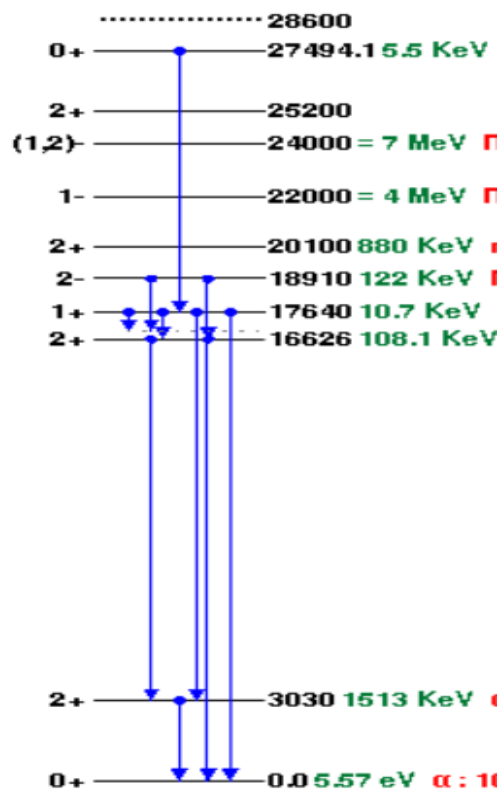
Number of charge carriers created is proportional to the energy of the incident particle. The energy loss  $dE/dx$  of incident particle is of interest follows bethe-bloch formula. The number of charge carriers created in the detector is proportional to the  $(dE/dx)t/e$  where  $t$  is the thickness and  $E$  energy requires to create one charge carrier. The particle passes through the delta detector and a signal proportional to the  $dE/dx$  will be observed and retaining most of its initial energy. It is possible to accept only those events that occur in the coincidence with the thick detector and thin (  $\Delta E$ ) detector. This allows a simultaneous measurement of  $dE/dx$  and  $E$  for each incident particle. They will be arranges as shown in fig 2.

## OBSERVATION

In this experiment, it is important to know the iso-spin of an excited state of the nuclei. Since, it will give us information about the transition and the reason behind it. Therefore, certain no core shell model calculations were done using NCSM code.

### NCSM calculation for $^8\text{Be}$

Preliminary calculations for  $^8\text{Be}$  nucleus have been performed using no core shell model (NCSM). The level scheme, up to the excitation energy  $\sim 20$  MeV, obtained with NCSM agrees reasonably well with the measured one. The maximum deviation between the calculated and the measured ones is less than 1 MeV. The NCSM reproduces very well the values for spin and the parity  $J^P$  as assigned experimentally. However, the total isospin assigned by experiment does not match with the NCSM predictions. Of particular interests are the  $1^+$  states at 17.6 MeV and 18.2 MeV which are responsible for the production of the new bosons as discussed above. These states are assigned a total isospin of  $T=1$  and  $T=0$ , respectively. The NCSM models yields  $1^+$  states at 18.5 and 18.8 but with opposite values of total isospins  $T=0$  and  $T=1$ , respectively. The following is the decay level of  $^8\text{Be}$  that is obtained from nndc.



## OBSERVATION

In the present experiment, we are interested in observing the electron positron pair and photon of  $\sim 20$  MeV respectively. The energy of these might range from 5 MeV to 20 MeV though essentially, the electron will be incident of the energy equivalent to 10 MeV which will help in understanding the physics of our interest. It thus becomes important to detect these particles efficiently.

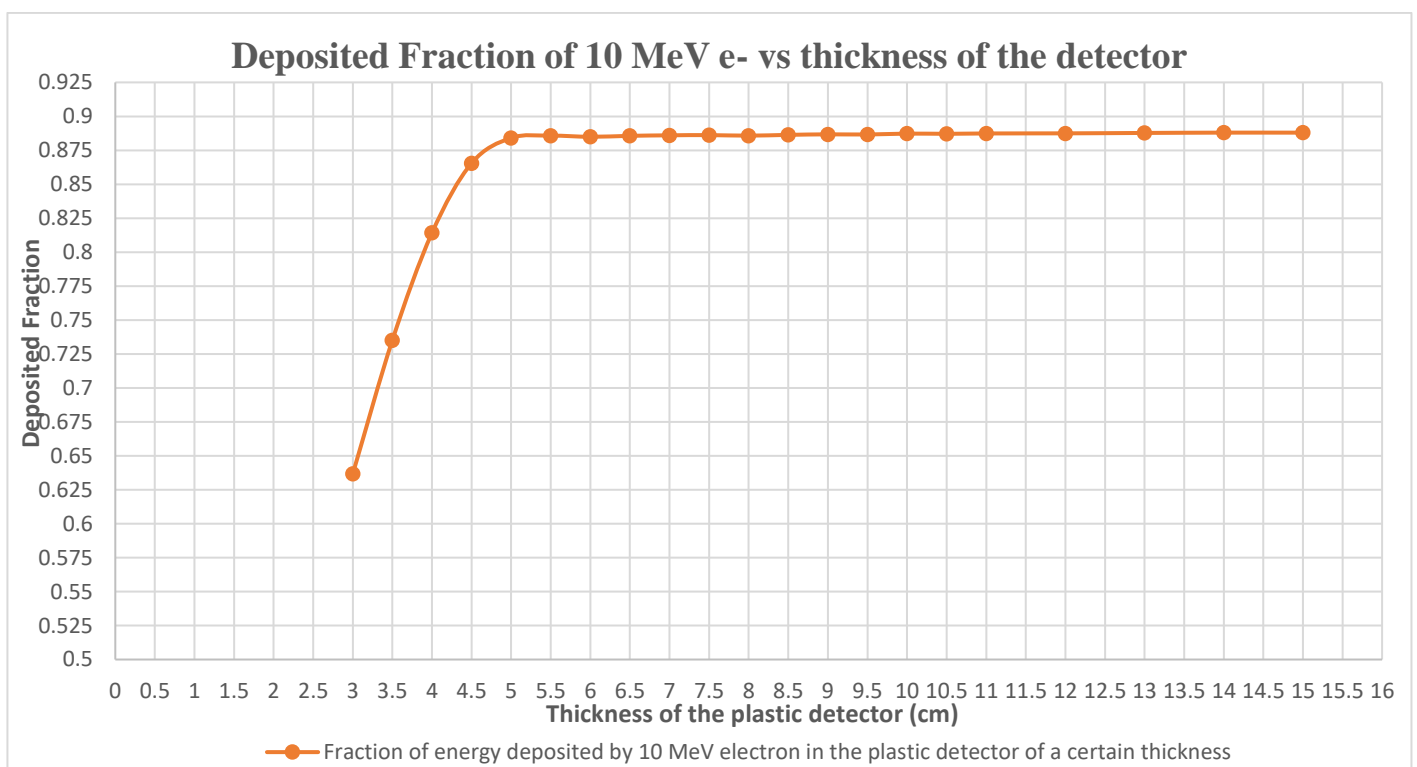
We tried to determine the efficiency of the detector by varying the thickness so as to determine the optimum thickness of the detector. Later once after determining the thickness, the energy of the electron and photon was changed to see how the detector responds to it. All the simulation were done using the EGS (Electron Gamma Shower) which is a Monte Carlo based simulation.

The results were first obtained for the plastic detector and later for the CsI scintillator detector so as to know which one is more efficient and is fit for our experiment.

The plastic detector that was considered was one with a base Polyvinyl Toluene. It has 9 C and 10 H and a density of the 1.032 g/cc. The data file for the cross-section was generated using the EGS. The geometry considered was a box with dimensions:  $(3.0 * 3.0 * t)$  cm, where  $t$  is the thickness. The mono – energetic electrons were thrown from the source along the  $z$ - direction, which was positioned on the surface of the detector.

### A. Using Plastic Scintillator Detector

Firstly, we tried to determine an effective thickness of the E type plastic detector for a 10 MeV  $e^-$ .

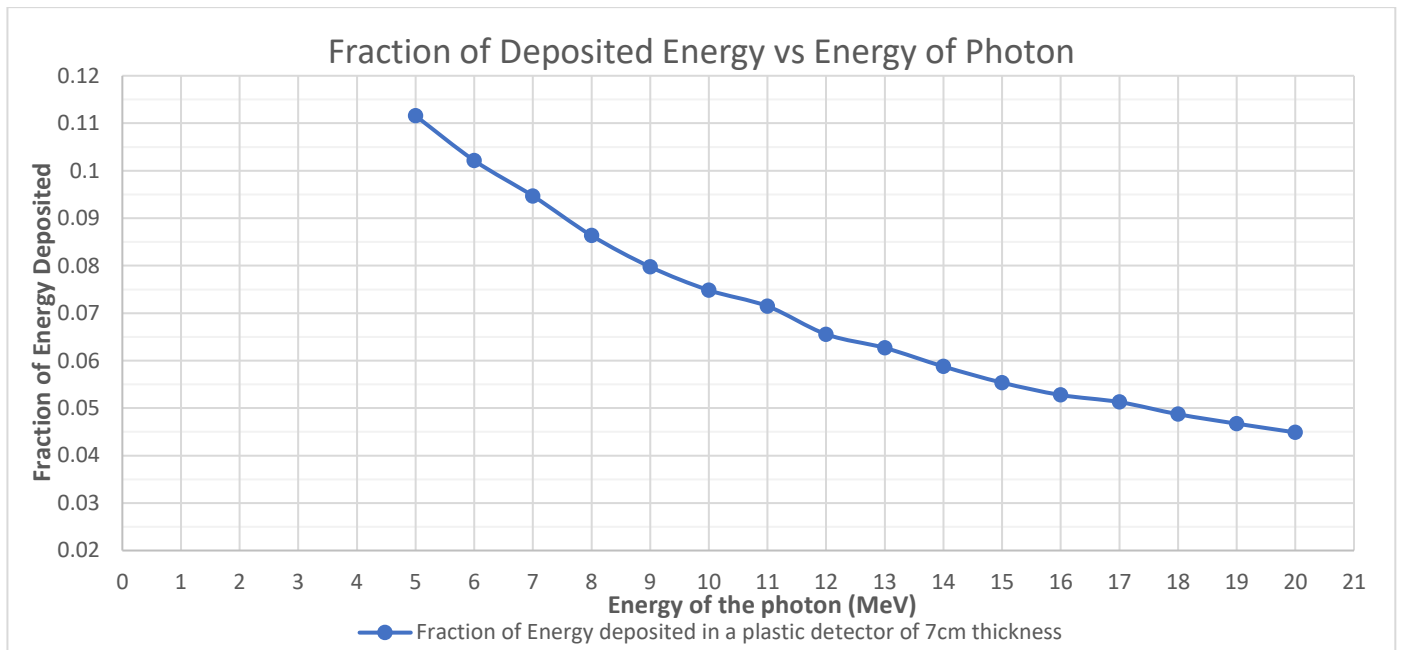


Graph 1

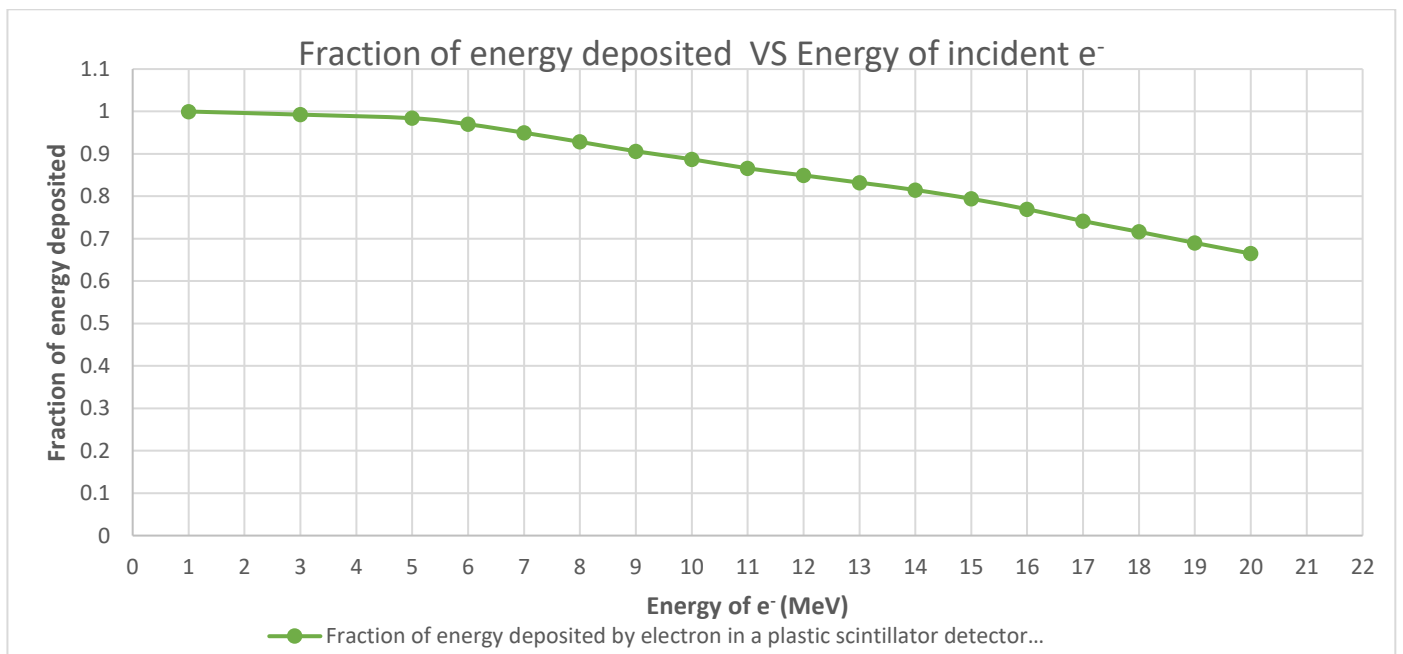
The dimensions that were used while simulating the detector :  $3.0 * 3.0 * t$  where  $t$  is the thickness which was varied. It can be seen that for a cube plastic detector of side 3.0 cm the efficiency is only 63 %, on increasing the thickness of the detector ; more energy is deposited in it as the shower starts confining it. After 5 cm the efficiency becomes almost constant equivalent to 88%. It never increases beyond 90%. This shows that a photon might be escaping from the detector.

This helped us in fixing the dimension of the plastic detector to be : **3.0 cm \* 3.0 cm \* 7.0 cm.**

Since, in the concerned experiment electrons and positron pairs are expected to be formed alongwith, the emission of photons or gamma rays from the de-excitation therefore, it becomes important to understand the behavior of the photons as well. For this purpose, simulations were done for a plastic scintillator by fixing its thickness to 7cm as shown in Graph 2.



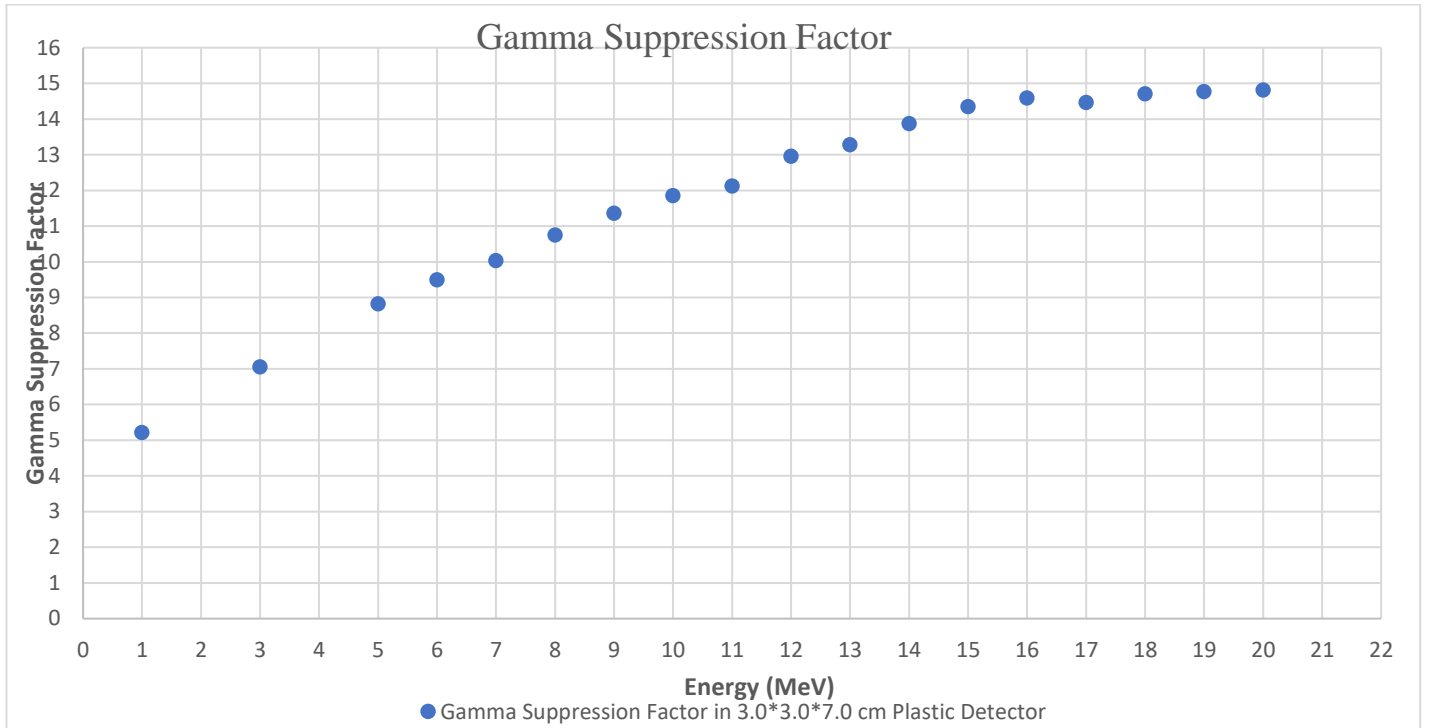
Graph 2



Graph 3

It was also simulated to see the fraction of energy deposited by various energed electron in the plastic detector. It can be inferred from the graph 3 that the deposition by the photon is maximum 1.1 MeV. The 1 MeV electron deoposits its entire energy in the detector. While, 10 MeV electron deposits 90% of its energy in it.

Similarly, suppression factor for the photons was estimated for this configuration and the following plot was obtained as shown in graph 4.

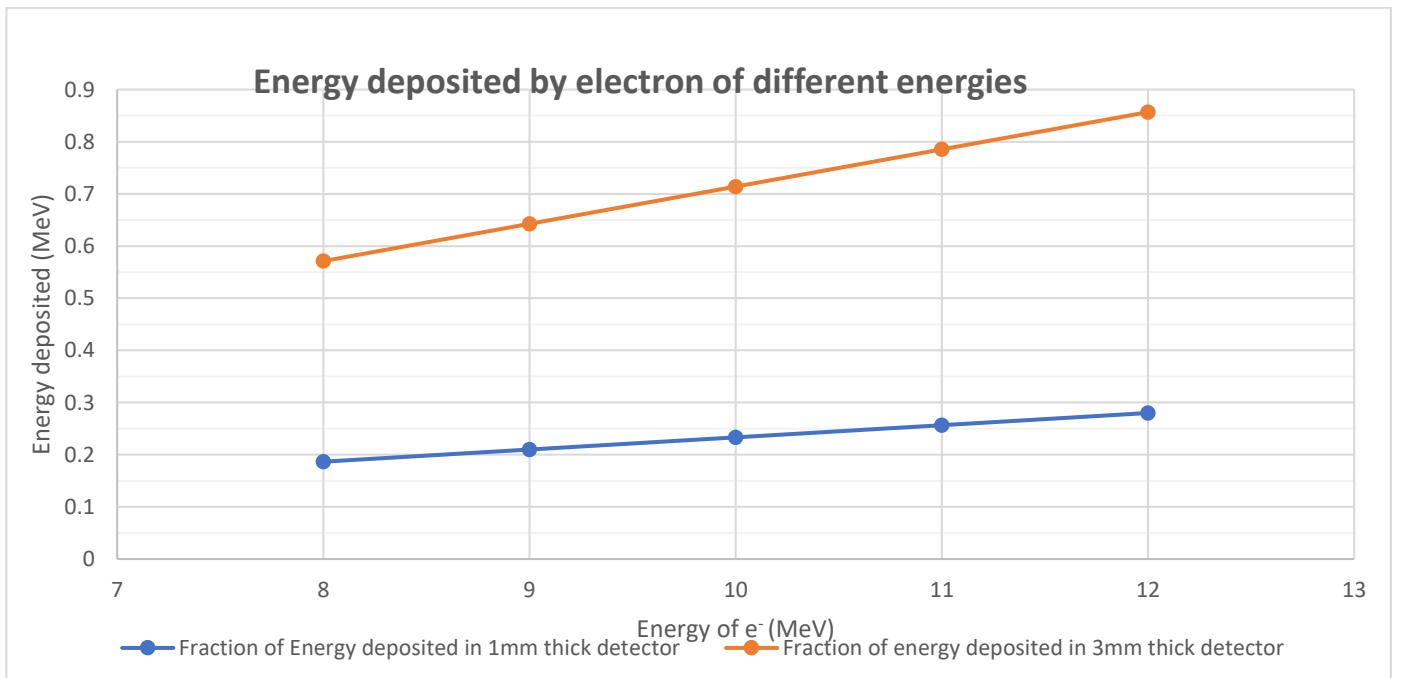


Graph 4

The gamma suppression factor was calculated by dividing the Efficiency of electron to efficiency when gamma is measured. It came out to be around 15 for the E detector as seen in graph %.

This fixed the dimension for the E detector to be  $3.0 \times 3.0 \times 7.0 \text{ cm}^3$ .

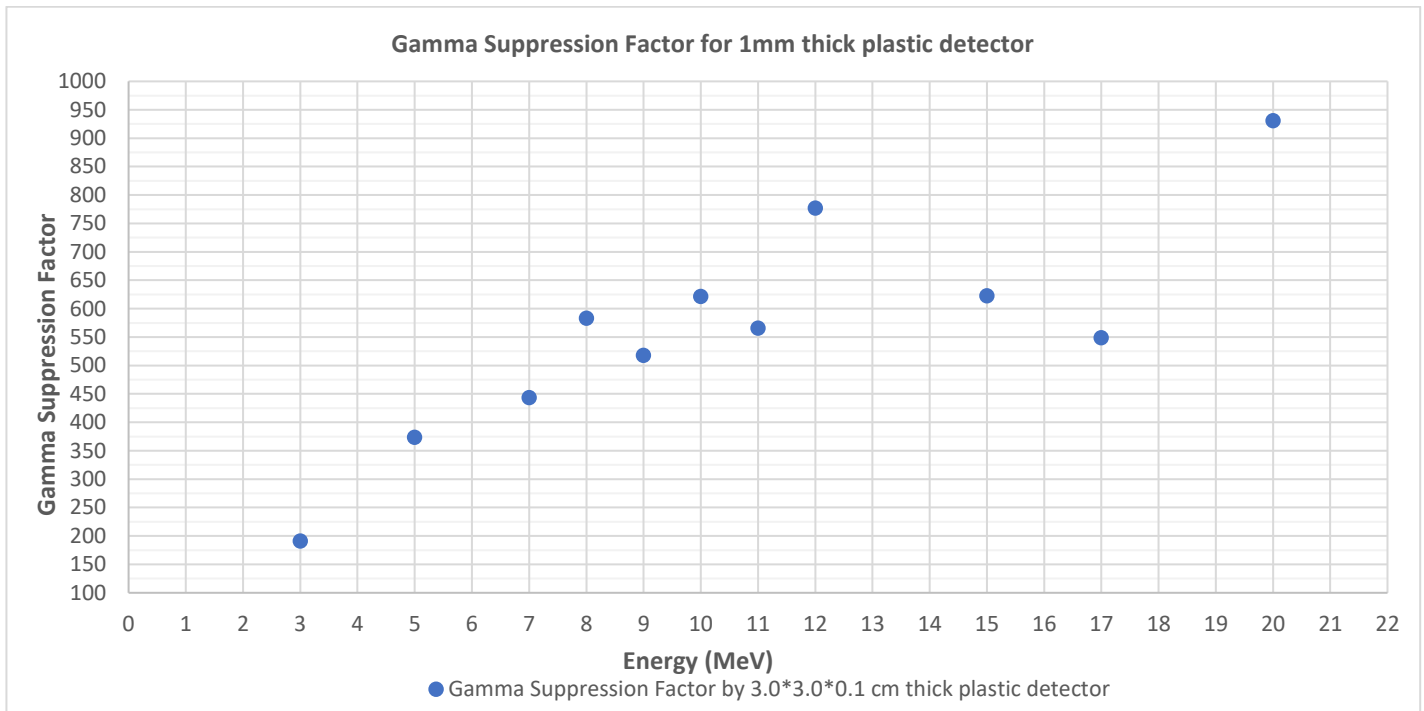
Similar exercise was also performed for the  $\Delta E$  detector of the dimension  $3.0 \times 3.0 \times 0.1 \text{ cm}$ . and  $3.0 \times 3.0 \times .3 \text{ cm}^3$ . The following is the graph of energy deposited by the electron in a delta E detector of different thicknesses.



Graph 5



It can be observed from the graph 5 that, only a small amount of energy is deposited in the plastic  $\Delta E$  detector. The energy deposited is 200 keV and 600 keV in 1mm and 3mm detector which matches with the literature[e]. Gamma Suppression for the small detector in the telescope setup as shown in graph 6.

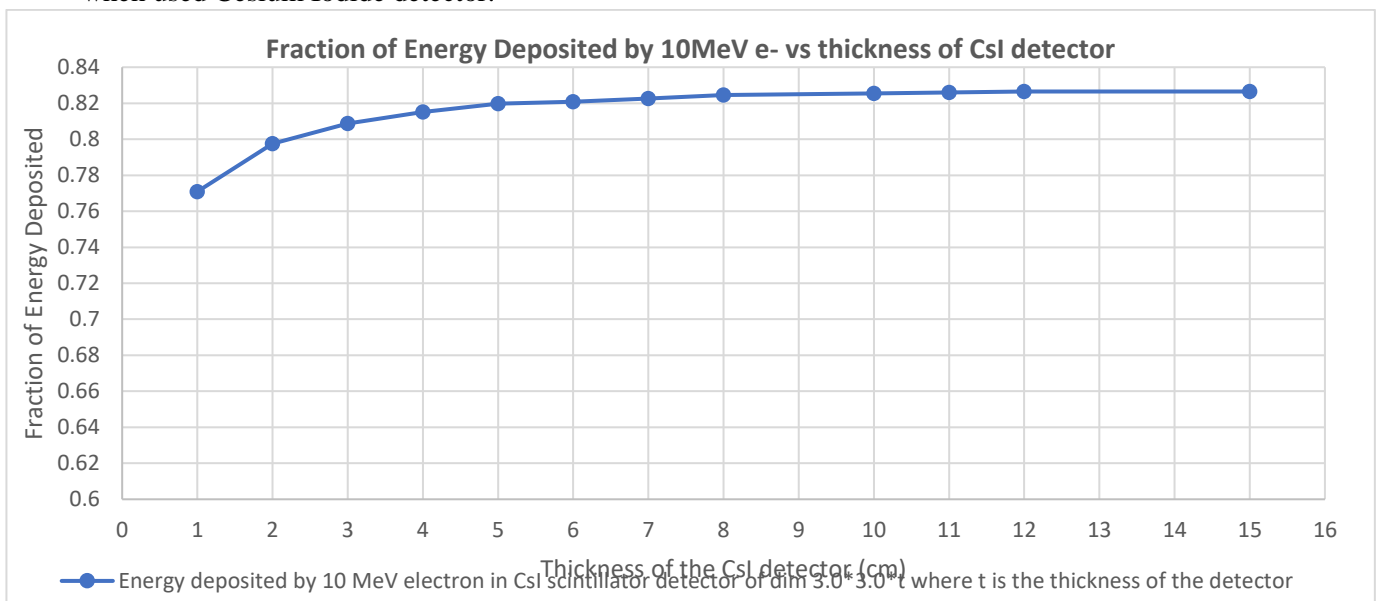


Graph 6

It can be seen from graph 6 that the plastic detector of the given configuration suppresses gamma rays compared to electron when both are of 10 MeV by 600 times. When combined together with the  $\Delta E$  detector we get a total gamma suppression of around 6000. This, hence validates the use of the plastic scintillator detector of the given dimensions for a particular experiment wherein we are more interested in detecting the electron positron pair

#### B. Using Cesium Iodide Scintillator Detector

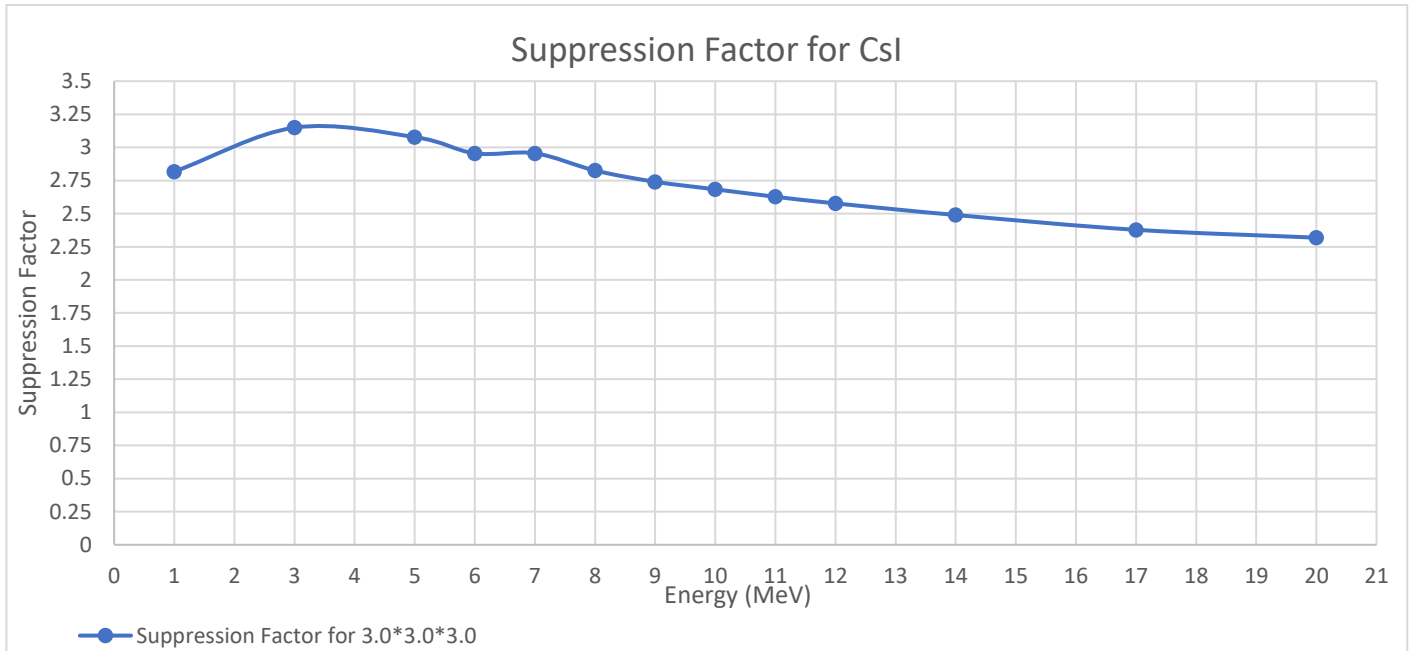
The similar exercise was also done so as to see how things change or the detection efficiency changes when used Cesium Iodide detector.



Graph 7

It was observed that the beyond 3 cm the efficiency was almost constant around 82 %. By keeping this in mind, a CsI detector can be designed for 3.0\*3.0\*3.0 cm thickness which will be more compact compared to the plastic detector.

If we were to use this detector in the experiment, it becomes important to obtain the gamma suppression factor by it. The simulations were done for photon and electron of 10 MeV when shot on the CsI detector of the config: 3.0\*3.0\*3.0 cm crystal, the following graph was obtained.



Graph 8

It can be seen that compression factor is ~3 for the CsI detector. One can also think of a prototype where one can use plastic scintillator as delE detector and CsI scintillator as E detector. This will make the detection system more compact keeping the accuracy same. It will be interesting to see how the spectrum changes when used this instead of the plastic detector as E detector.

### C. Designing of the detector and Testing

After doing the above-mentioned simulations. We finalised to design a (3.0\*3.0\*7.0 )cm<sup>3</sup> detector made out of seven 3.0\*3.0\*1.0 cm<sup>3</sup> cube tiles as shown in the fig 10. These were glued together to form one crystal. Later, the waveguide was attached at the end of the crystal as shown in fig 10 (b). The photomultiplier was attached using silicon grease to get a plastic detector as shown in fig 11.

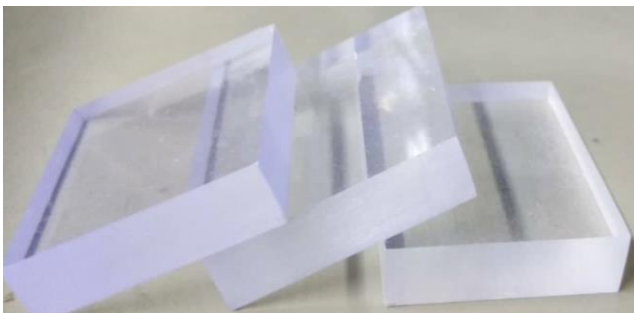


Fig 10 (a)



Fig 10(b)

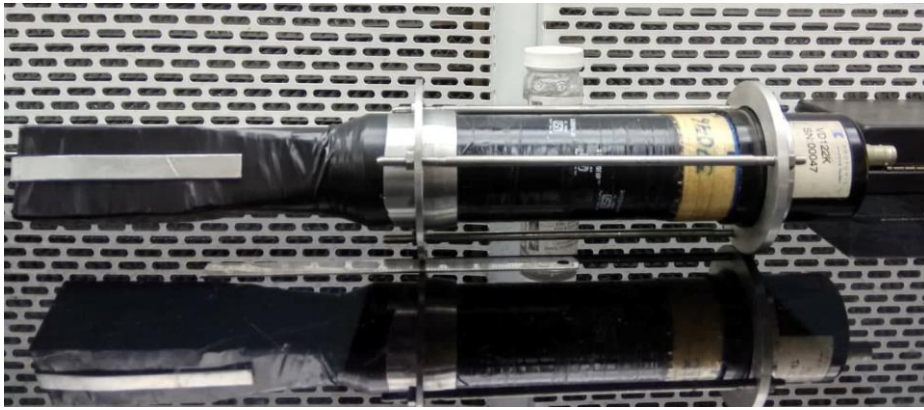


Fig 11

After the detector was designed, it was tested using the gamma sources in VECC. To our surprise, detector responded and worked in the first go itself. The following spectra were obtained for  $^{137}\text{Cs}$ ,  $^{60}\text{Co}$ ,  $^{22}\text{Na}$ , Am-Be source as shown in below.

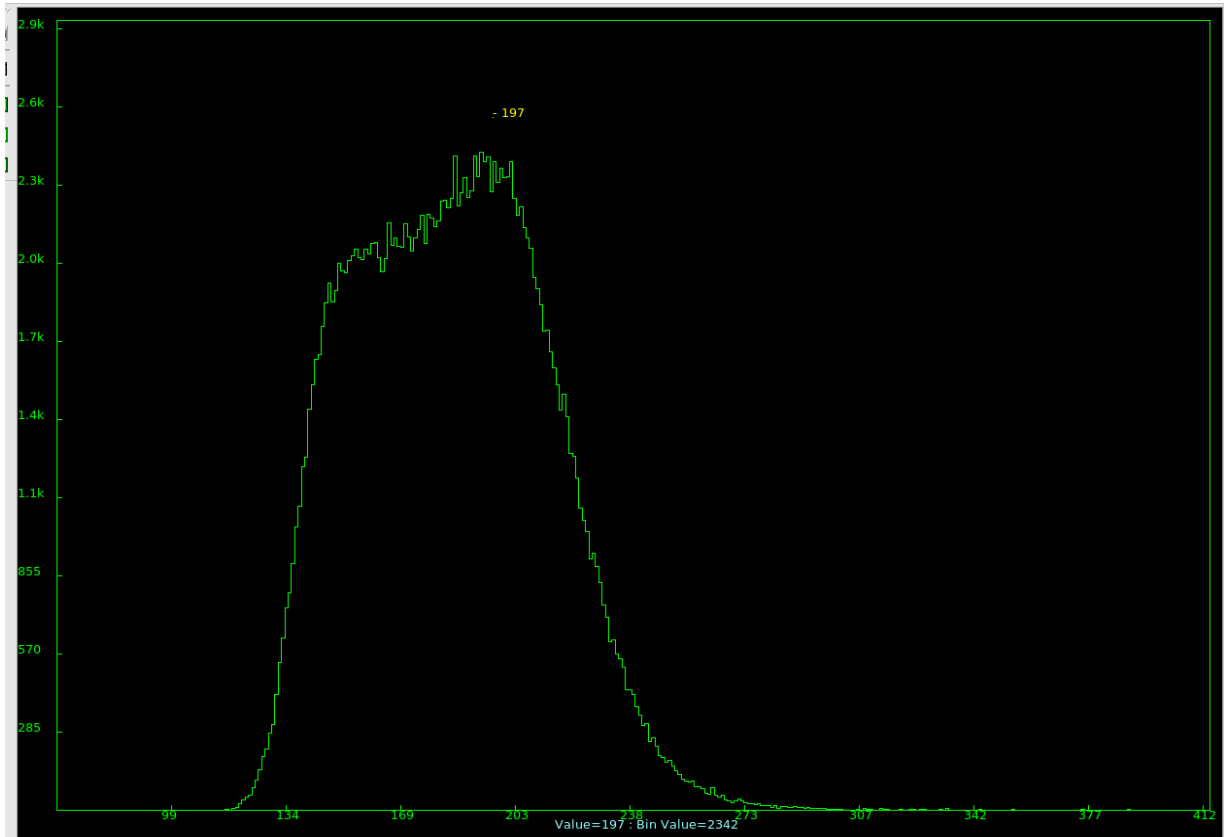


Fig 12 Spectrum of  $^{137}\text{Cs}$  from plastic detector that was designed.

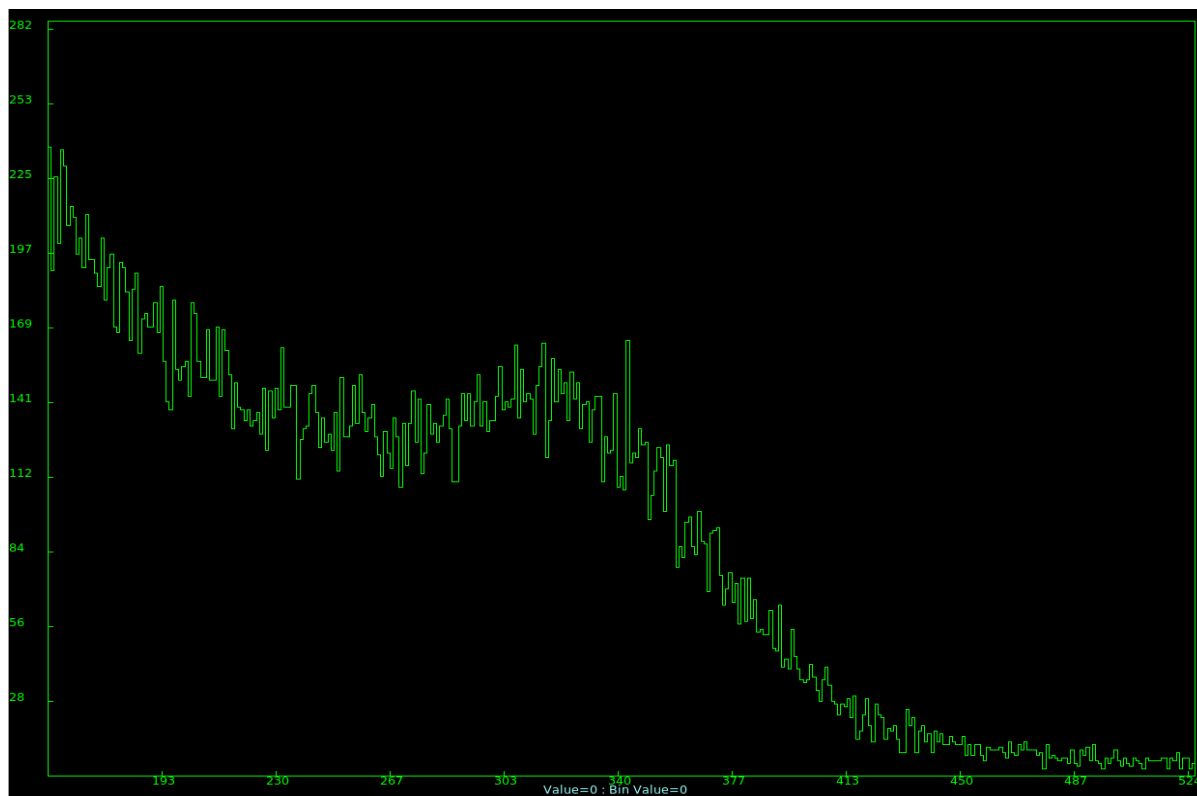


Fig 13  $^{60}\text{Co}$  spectrum

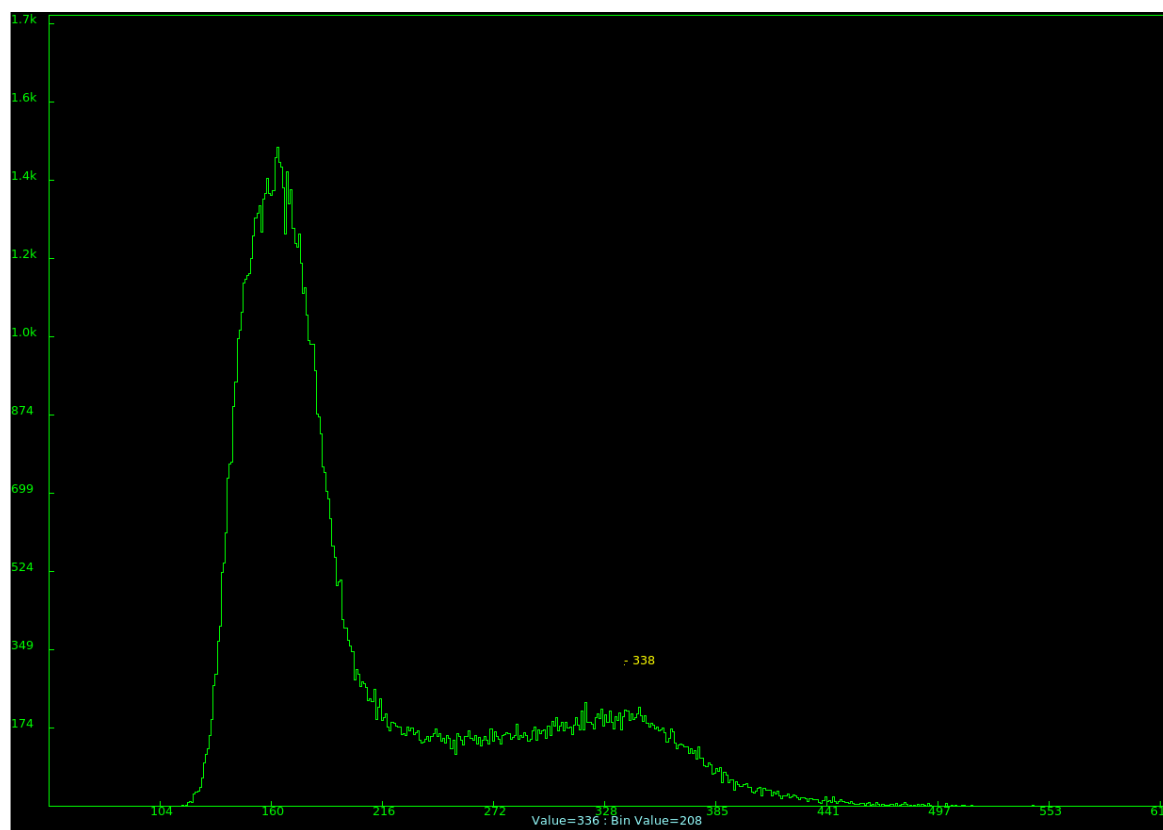


Fig 14  $^{22}\text{Na}$  spectrum

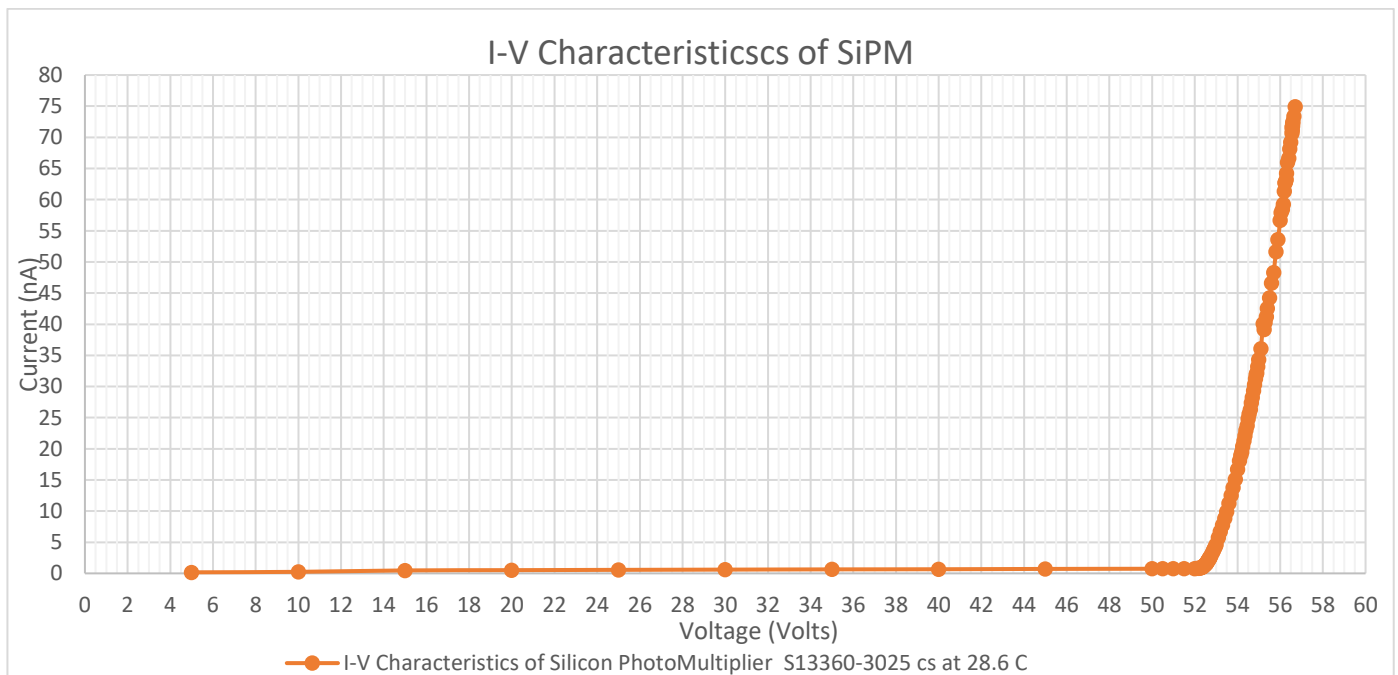
All these data were for low energy gamma rays of maximum 2 MeV. Therefore, to test for higher energy, we observed the energy deposited by the muon. It was arranged as shown in the figure \*\*. Since, the thickness of the detector is 3 cm in the direction of the muon flux. The energy deposited in the detector as per the simple calculation should be 6 MeV. Since, the muon flux is 1 muon per centimeter square per **second**. The following Is the table for the peak position observed and works out the calibration constants

Source	Energy (MeV)	Channel Number
<sup>137</sup> Cs	.667	197
<sup>60</sup> Co	1.250	314
<sup>22</sup> Na	1.220	338
Am-Be	4	923
	4.5	1030

This gives the calibration constant for  $y = mx + c$  where, y is the energy of the photopeak, x is the channel number at which the peak appears. This results in  $m = 216.5$  and  $c = 56.48$ .

### Using Si-Pm

In our next prototype we plan to put Si-PM( Silicon Photo Multiplier) to convert the photons into electrical signal. This will make the whole detection system compact. Before the Si-Pm is connected to the crystal it is important to study its I-V characteristics to know it's operational voltage (i.e the voltage at which it should be operated). Other parameters like, dark current and break-down voltage were also determined. The SiPM was reverse biased.



Graph 9

It can be seen from the graph 9t that the breakdown voltage for SiPM Hamamatsu S13360-3025 CS (Multi Pixel Photon Counter) is 52.42 V. The operating voltage is 56.65 V and the dark current is 73.4 nA. The following spectra were obtained at different voltages so as to fix at which voltage the SiPm should be operated such that it resolves the peak and is efficient as well as shown in fig 15 to fig 19.

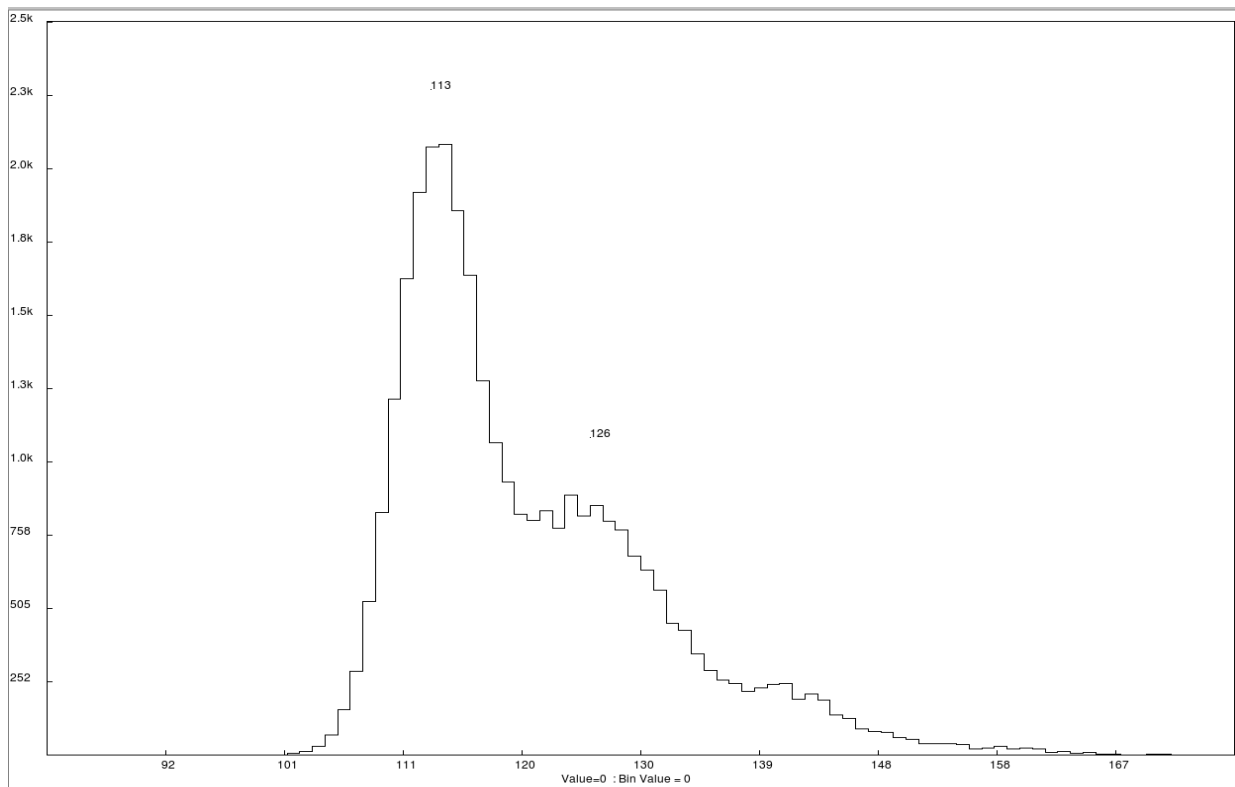


Fig 15 The spectrum obtained from the SiPM when operated at 53.4 V 1

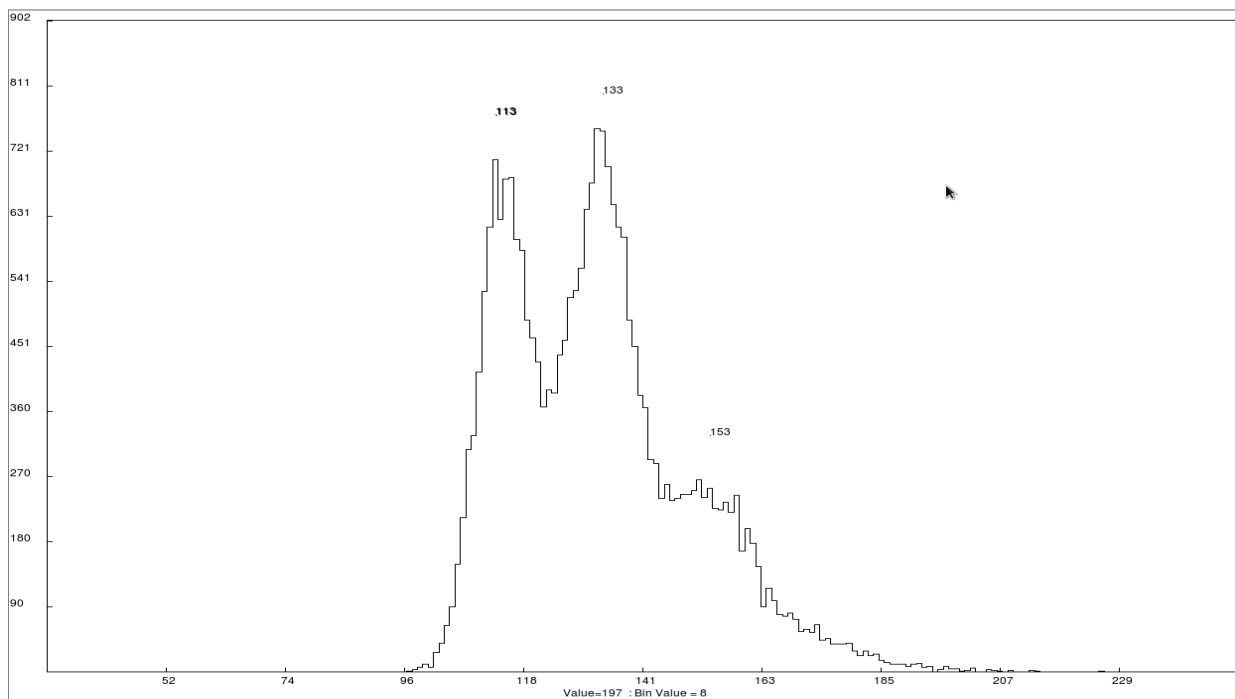


Fig 16 The spectrum obtained from the SiPM when operated at 53.9 V

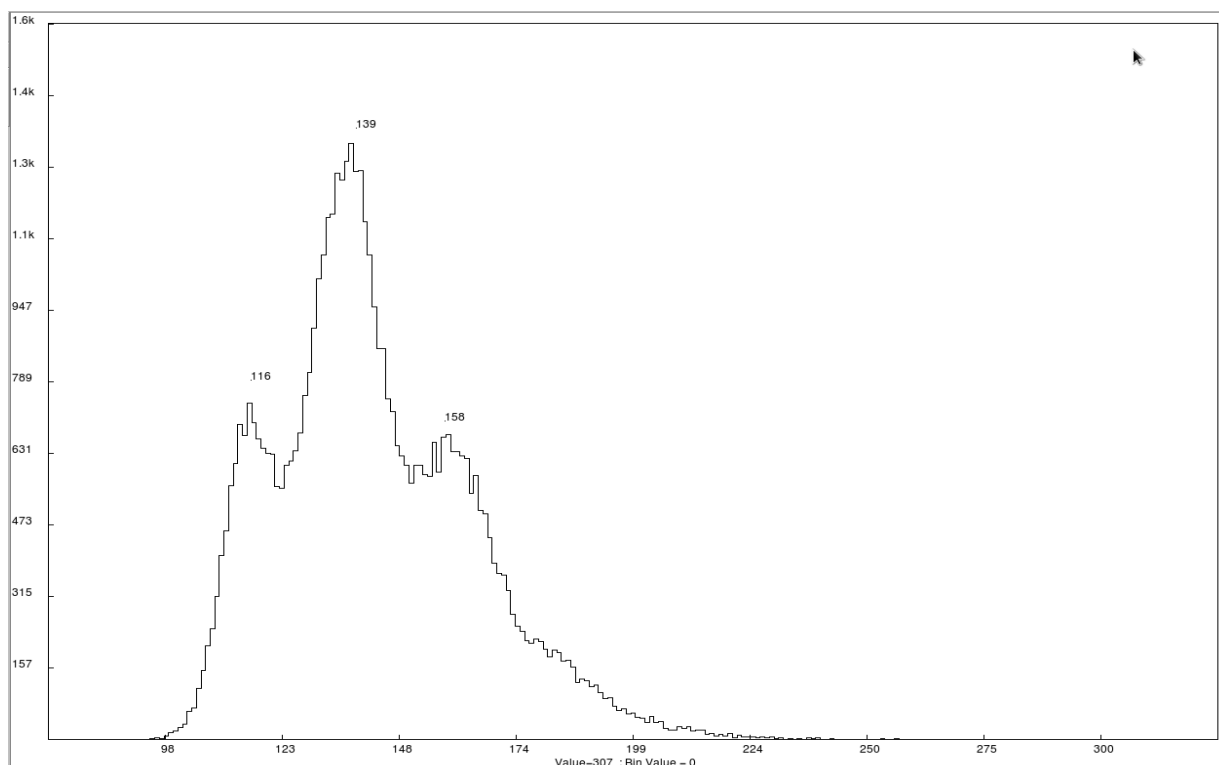


Fig 17 The spectrum obtained from the SiPM when operated at 53.4 V

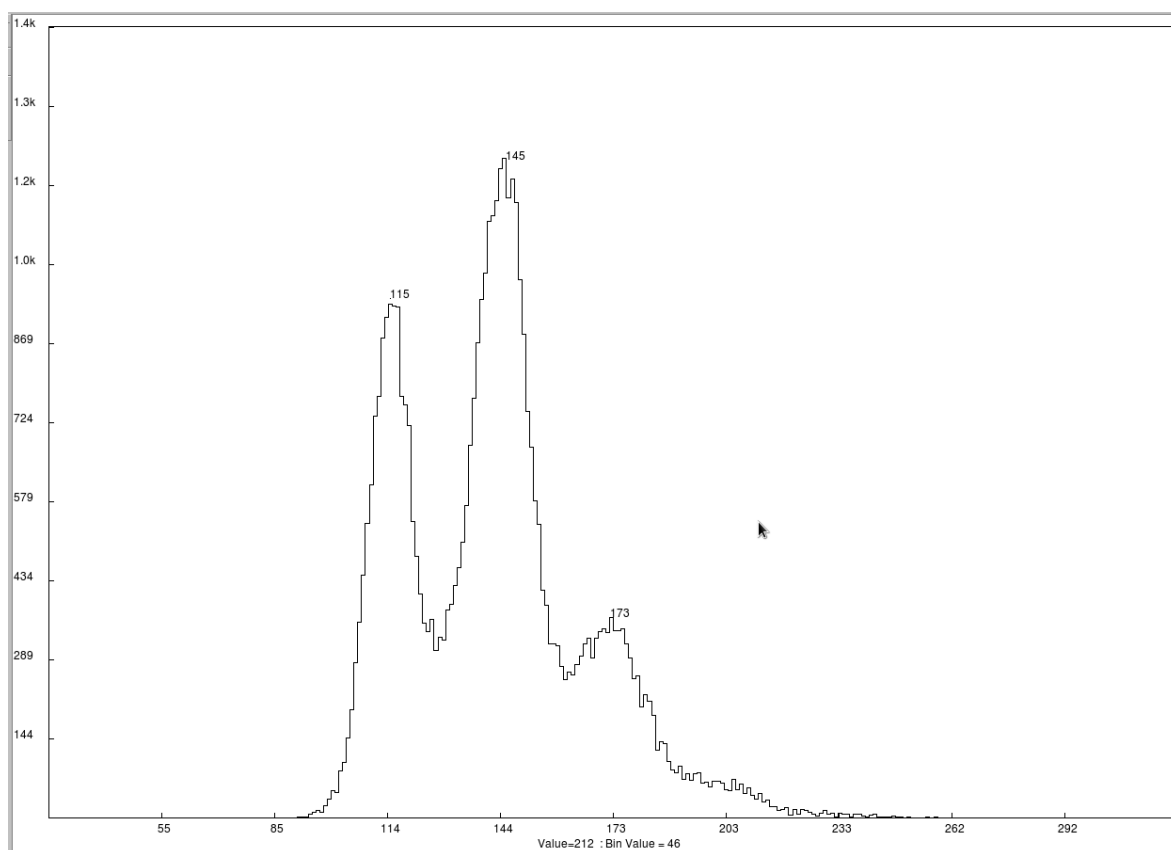


Fig 18 The spectrum obtained from the SiPM when operated at 54.4 V

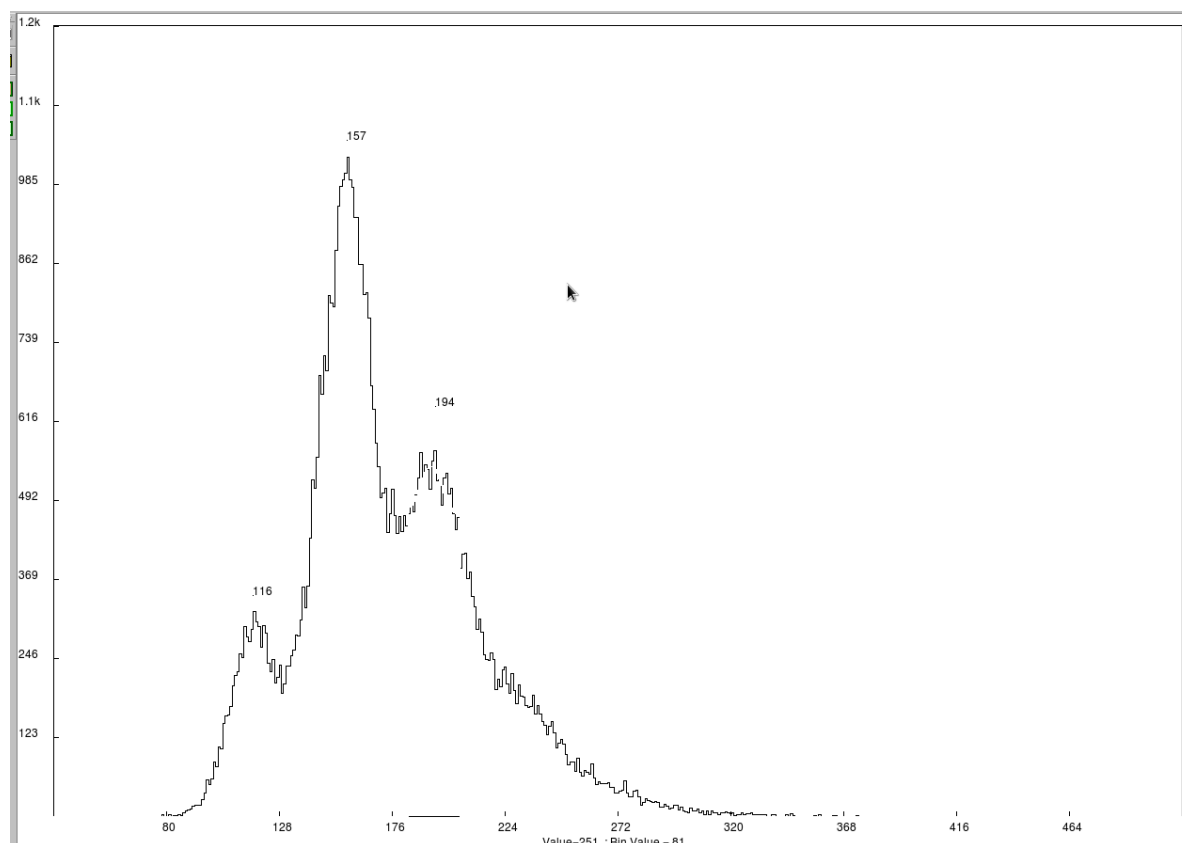


Fig 19 The spectrum obtained from the SiPM when operated at 55.4 V

It can be seen from the above spectra that on increasing the operating voltage the peaks are better resolved upto 54.4 V and the resolution and the efficiency decreases when the voltage is increased further. It can be seen from the following table which shows the peak position and the resolution at a particular voltage. It is interesting to note that as the voltage is increased the number of channels between the peak increases from by 10 channels. The peaks correspond to the first escape and second escape of photon. Therefore, the SiPM should be operated at 54.4 V.

## **CONCLUSION**

In the current project, an attempt was made to understand the reason behind such a decay to boson in nuclear transition. Since, it is not yet clear if it is iso-scalar boson or iso-vector boson which are differently claimed by two experimental group; it therefore, is important to know the characteristic of this boson. In this regard, it is important to know the iso-spin of the states for which we did some NCSM calculations for  $^8\text{Be}$ .

Besides theory, it is important to make the experimental set up better and more efficient for which initially a simulation was done using EGS to optimize the dimension of the detector and the material that should be used. After, simulating the dimensions were fixed to be as  $3.0 \times 3.0 \times 7.0 \text{ cm}^3$  for the plastic detector which is 88% efficient. Similarly for CsI the dimensions were fixed as  $3.0 \times 3.0 \times 3.0 \text{ cm}^3$ . Since, we are interested in the  $e^- e^+$  pair; a delta E detector will also be used of thickness 0.1 cm.

After fixing the dimensions the plastic scintillator detector was designed of 7cm thickness with a PMT attached and was tested using different sources. In another prototype, we plan to attach SiPM which can be used in the external magnetic field as well which will be used to make the setup more effective, as the  $e^- e^+$  pair will behave differently in the mag field and make the detection system more efficient.



**Plans:**

- 1) Shell model calculations for estimating the different states, transition rates and isospin.(ongoing work)
- 2) Simulation, setting up and testing of prototype detector with conventional photomultiplier and Silicon Photomultiplier. (ongoing work)
- 3) Experimental verification with the existing accelerators at Delhi and Mumbai
- 4) Setting up magnetic spectrometer, detector setup for these measurements.
- 5) Contributing towards setup for gaseous targets, beam lines,  $^3\text{He}$  beams for experiments at FRENA.

## **REFERENCE**

[1] A. J. Krasznahorkay, M. Csatlós, L. Csige, Z. Gácsi, J. Gulyás, M. Hunyadi, I Kuti, B. M. Nyakó, L. Stuhl, J. Timár, T. G. Tornyí, Zs. Vajta, T. J. Ketel and A. Krasznahorkay PRL 116, 042501 (2016)

[2] Jonathan L. Feng, Bartosz Fornal, Iftah Galon, Susan Gardner, Jordan Smolinsky, Tim M. P. Tait, and Philip Tanedo PRL 117, 071803(2016)

[3] K.E Stielbing, de Boer, O Frohlich, K A Muller, Journal of Physics, Nov 2003.

[4] F.W.N. de Boer a,1, O. Fröhlich, K.E. Stiebing”, K. Bethge a, H. Bokemeyer , A. BalandaC, A. Budadye, R. van Dantzig f, Th.W. Elze a, H. Folger, J. van Klinkend, K.A. Miiller ‘, K. Stelzer ‘, M. Waldschmidt PLB (1994)

[5] G. A. Fisher, P. Paul, F. Reiss, Phys. Rev C 14,28 (1976)